Applied Physics A (2021) 127:
https://doi.org/10.1007/s00339-021-04455-3

**Applied Physics A**
**Materials Science & Processing**

# Analytical model for the depth progress of percussion drilling with ultrashort laser pulses

**Daniel Holder[1,1] · Rudolf Weber[1] · Thomas Graf[1] · Volkher Onuseit[1] · David Brinkmeier[1,2] · Daniel J. Förster[1,3] · Anne Feuer[1]**

Received: 1 February 2021 / Accepted: 19 March 2021 / Published online: 2 April 2021


**Abstract**
A simplified analytical model is presented that predicts the depth progress during and the final hole depth obtained by laser percussion drilling in metals with ultrashort laser pulses. The model is based on the assumption that drilled microholes exhibit a conical shape and that the absorbed fluence linearly increases with the depth of the hole. The depth progress is calculated recursively based on the depth changes induced by the successive pulses. The experimental validation confirms the model and its assumptions for percussion drilling in stainless steel with picosecond pulses and different pulse energies.

**Keywords** Percussion drilling · Metals · Ultrashort laser pulses · Depth progress · Analytical model

## 1 Introduction

For the manufacturing of parts such as dry metal forming tools with lubricant holes [1] and spinneret nozzles for direct spinning of micro-fibers, efficient drilling of several hundred of high-quality microholes is required in hardened deep drawing tools [2] and spinnerets [3], respectively. Helical drilling with ultrashort laser pulses is often used for a defined shaping of high-quality microholes [4–6]. However, this approach requires special cost-intensive optics. In contrast, percussion drilling can be performed with a simple setup and allows for efficient and productive drilling of microholes with a high drilling rate and short breakthrough times, which is important when several hundreds of microholes need to be drilled into one workpiece. Short drilling times in metals can be achieved by percussion drilling at repetition rates in the range of hundreds of kHz or MHz [7–9]. However, the drilling rate at high repetition rates is increased by excessive melt formation [7, 10, 11] due to heat accumulation effects [12, 13]. Melt formation significantly reduces the hole quality, e.g., with the formation of rims at the hole inlet [7, 9, 11] and recast layers within the hole [9]. Quality reducing effects can also occur at lower repetition rates when high fluences are used. In this case, the occurrence of a particle-ignited plasma causes a widening of the hole entrance [14, 15] and bulge formation within the hole [16]. The excessive generation of melt and the formation of particle-ignited plasma during laser drilling must be avoided for demanding applications such as the manufacturing of the mentioned lubricant holes in dry metal-forming tools in order to achieve high-quality microholes and maintain the specific properties of the hardened deep drawing tool.

Conical hole geometries are formed during percussion drilling with ultrashort laser pulses [9, 16–19] as long as the thermal defects are avoided. Following *Döring* et al., the evolution of the hole's depth during percussion drilling can be divided into three distinct phases:

In phase 1, the drilling process is mainly characterized by a high drilling rate and results in a reproducible hole geometry. The drilling process in phase 2 is dominated by an irregular drilling progress with gradually decreasing drilling rate and decreasing reproducibility of the hole geometries. Finally, in phase 3, the drilling process is defined by stagnation with a ceasing drilling progress [20]. Hence, each phase exhibits different drilling rates and hole qualities, as described in [20] for drilling in silicon. The three

✉ Daniel Holder
daniel.holder@ifsw.uni-stuttgart.de

[1] Institut für Strahlwerkzeuge (IFSW), University of Stuttgart, Pfaffenwaldring 43, 70569 Stuttgart, Germany

[2] Graduate School of Excellence Advanced Manufacturing Engineering (GSaME), Nobelstraße 12, 70569 Stuttgart, Germany

[3] LightPulse Laser Precision, Pfaffenwaldring 43, 70569 Stuttgart, Germany

phases may be interpreted as a superposition of a regular drilling process, that dominates in phase 1 and that continues in phase 2 and 3 but with a decreasing depth growth with increasing number of pulses, and irregular drilling contributions that start to become noticeable and later dominate the further depth growth as from phase 2. Hence, the evolution of the drilling depth may be described as a sum of the drilling depth achieved with the regular process and the additional depth generated by the irregular, i.e., unpredictable, contributions. Both contributions come to a stop in phase 3. Drilling of reproducible and conically shaped microholes can be achieved when the drilling process is stopped before the end of phase 1, where the drilling is still dominated by the regular process without noticeable influence of the irregular contributions, which led to the definition of a "quality depth limit" [16, 20]. An analytical model for the estimation of the quality depth limit of percussion drilling with picosecond laser pulses is presented in [16]. Drilling deeper than the quality depth limit is not efficient due to the gradually decreasing drilling rate and stagnation in phase 2 and phase 3, respectively [20]. In addition, the depths obtained in the phases 2 and 3 are increasingly affected by the irregular drilling contributions. Therefore, it is essential to know the drilling rate at any time during the percussion drilling process when efficient drilling of reproducible and conically shaped microholes is required. Optical coherence tomography was demonstrated to be a versatile tool for online monitoring of the ablated depth [21, 22] or drilling rate during drilling with short and ultrashort laser pulses [23]. Appropriate processing of the OCT signals allowed for the determination of the hole depth with an accuracy of ± 30 µm during percussion drilling of stainless steel with nanosecond laser pulses [24].

An analytical model for the prediction of the *regular* drilling progress during laser percussion drilling through all the 3 abovementioned phases is introduced in the following. The model was experimentally verified using a calibrated OCT-based depth measurement for the case of drilling of blind holes with a depth of up to 1.5 mm in stainless steel with different pulse energies.

## 2 Depth progress and hole geometry of percussion-drilled microholes

The model presented in Sect. 3 is motivated by the experimentally observed depth progress and the resulting geometry of microholes that were percussion-drilled in stainless steel plates using picosecond laser pulses. The experiments presented in the following were performed in ambient atmosphere using the setup shown in Fig. 1.

The processed material was cold-rolled stainless steel of the type AISI 304. The processing laser with a wavelength of $\lambda_{Laser} = 1030$ nm and a pulse duration of 8 ps was operated at a low repetition rate of 21.4 kHz and the laser beam was circularly polarized. Optical measurements of the depth of the holes were performed with a Fourier-domain OCT-based system (CHRocodile 2, Precitec), which provides a measurement rate of 70 kHz, an axial measurement range of approximately 6 mm and an axial measurement accuracy of down to ± 1 µm. The processing laser beam and the OCT probe beam were coaxially superposed by means of a dichroic mirror (Layertec), which was HR-coated for the beam of the processing laser at a wavelength of $\lambda_{Laser} = 1030$ nm and AR-coated for the OCT beam centered at a wavelength of $\lambda_{OCT} = 1080$ nm. The beams were guided through a Galvanometer-scanner for deflection and focused by an F-Theta lens with a focal length of $f = 340$ mm, resulting in focal radii of $w_0 = 61 \pm 5$ µm for the processing laser and of $15 \pm 5$ µm for the OCT probe beam. The OCT-based depth measurements were recorded during the experiments and analyzed after applying two numerical signal-processing filters. First,

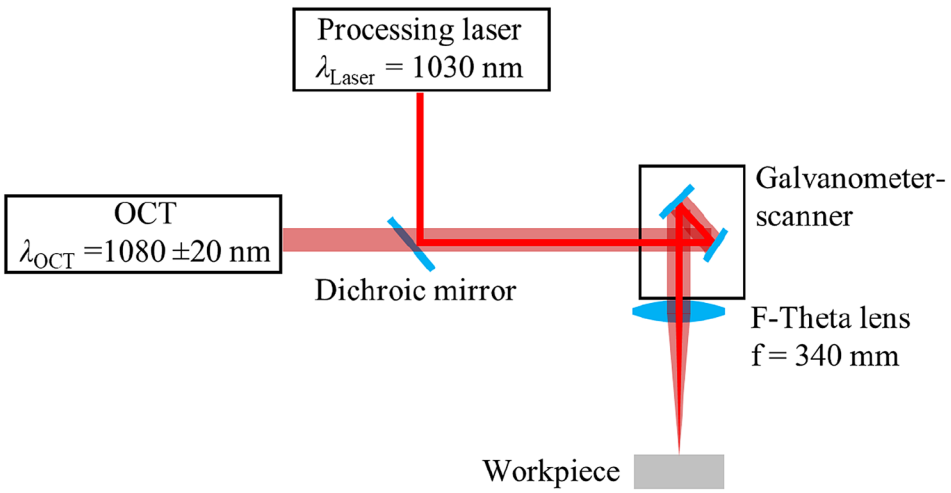


**Fig. 1** Experimental setup for the OCT-based measurement of the depth of the holes during laser percussion drilling

a signal-to-noise ratio (SNR) filter was applied in order to remove noise. Second, an "increasing depth"-filter was applied to the SNR-filtered values. This filter is based on the assumption that the hole depth can only increase and not decrease by drilling with ultrashort laser pulses and low repetition rates as shown in [23]. Hence, only the depth values for which the newly measured depth is larger than the previously determined depth are considered. Application of both filters and linear interpolation between the depth values yields the evolution of the drilling depth as a function of the number of incident pulses.

Figure 2 shows a filtered OCT-based depth measurement of the percussion drilling progress as a function of the number of pulses (red line) for a pulse energy of $E_p = 143$ µJ. Six holes were drilled using the same energy $E_p = 143$ µJ but with different total numbers of pulses for the verification of the OCT-based depth measurements by means of cross sections of the holes. The micrographs of these cross sections of holes produced by the application of 10,000 (inset no. 1), 20,000 (inset no. 2), 50,000 (inset no. 3) and 75,000 (inset no. 4) pulses are shown in Fig. 2 with the corresponding depth values marked as blue squares. The light blue scale bar represents a length of 200 µm.

The hole depth measured by OCT increased with a high drilling rate during the first approximately 34,000 pulses until a hole depth of about 530 µm was reached, corresponding to phase 1 of the drilling process. For higher numbers of pulses, the growth of the depth achieved by the regular drilling process slows down and finally saturates and the further growth of the hole is characterized by the irregular contributions in phase 2 and 3. A similar behavior was found for drilling of silicon [20]. The deviations between the depths measured by OCT and the depths obtained from the cross sections shown in the micrographs might result from inaccuracies of the OCT-based depth measurement [24] or more probably to the inaccuracy of the grinding /polishing process used for the creation of the cross sections. As the center of the hole is not easily hit during grinding and polishing, the depth determined from these cross sections systematically yield a value that is too small. Nevertheless, the cross sections provide important information about the shape of the hole. For percussion drilling of stainless steel with picosecond pulses with a pulse energy of $E_p = 143$ µJ, a focal radius of $w_0 = 61$ µm, and up to a total of 75,000 pulses (inset no. 4), the conical hole shape clearly dominates the geometry of the drilled holes, indicating a drilling process within the "quality depth limit" [16].

## 3 Analytical model of the depth progress during percussion drilling of conically shaped microholes

Based on these findings, an analytical, recursive model was derived for the calculation of the depth progress that is achieved by the *regular* drilling process. The recursive model is based on the assumption that the hole depth $z_{hole,n}$ after $n$ pulses can be calculated by

$$z_{\mathrm{hole,n}} = z_{\mathrm{hole,n-1}} + z_{\mathrm{abl,n}}, \tag{1}$$

where $z_{\mathrm{hole,n-1}}$ denotes the hole depth after $n$-1 pulses, $z_{abl,n}$ denotes the depth ablated by the $n^{\mathrm{th}}$ pulse, and $n \in 1, 2\ldots N$. For the shape of the hole, the simple geometrical

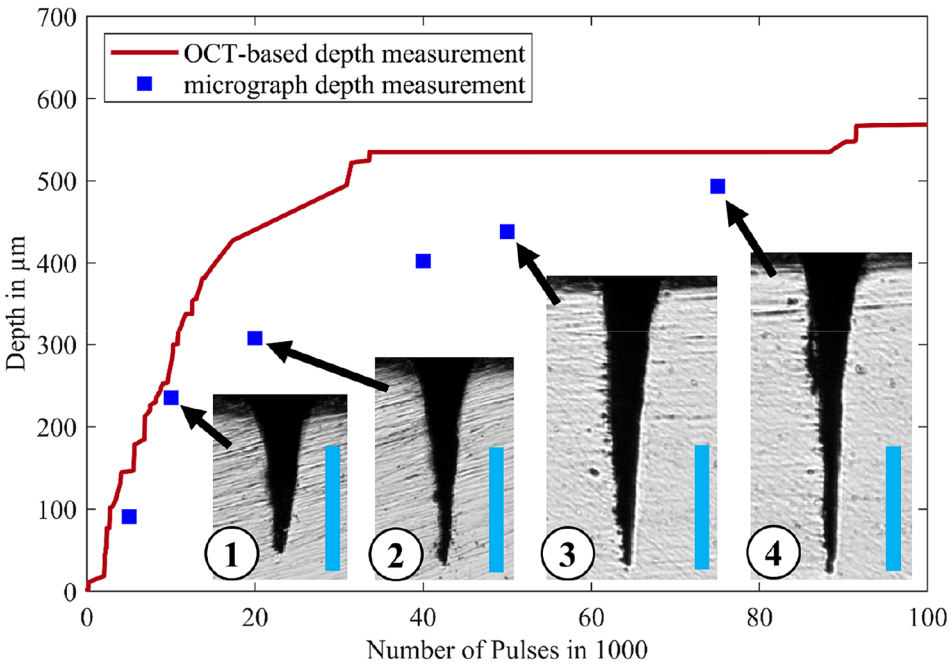


**Fig. 2** Hole depth as a function of the number of applied pulses as measured by OCT (red curve) and as measured from micrographs of cross sections (blue squares). The percussion drilling was performed with a pulse energy of $E_p = 143$ µJ and a focal radius of $w_0 = 61$ µm. Corresponding cross sections of some of the holes drilled with 10,000 (1), 20,000 (2), 50,000 (3), and 75,000 (4) pulses are shown as insets. The light blue scale bars with the insets represent a length of 200 µm

approximation of a cone is assumed, as illustrated in Fig. 3. This corresponds to the experimental results shown in Fig. 2, where the geometry of a high-quality hole is typically of conical shape.

The radius $r_{hole}$ of the hole´s opening drilled with a Gaussian beam is determined by the ablation threshold fluence $\Phi_{abs,th}$ and is given by [16, 25]

$$r_{\mathrm{hole}} = w_0 \cdot \sqrt{\frac{1}{2} \ln\left(\frac{\Phi_{\mathrm{abs},0}}{\Phi_{\mathrm{abs,th}}}\right)} \tag{2}$$

where $\Phi_{\mathrm{abs},0}$ denotes the absorbed peak fluence on the flat workpiece at the center of the Gaussian beam at normal incidence and $w_0$ is the radius of the beam on the surface of the workpiece. The absorbed peak fluence is given by

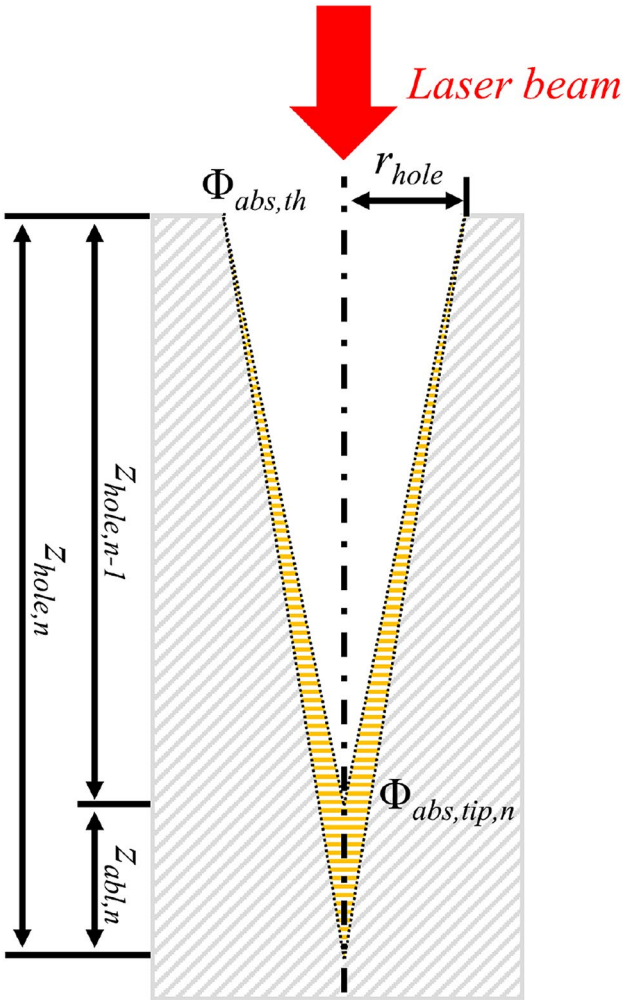


**Fig. 3** Cross section of a cone-shaped hole with an entrance radius $r_{\mathrm{hole}}$ and a depth of $z_{\mathrm{hole,n}}$ after the application of the $n^{\mathrm{th}}$ pulse. The absorbed fluence of the $n^{\mathrm{th}}$ pulse in the hole is assumed to linearly increase from $\Phi_{\mathrm{abs,th}}$ at the entrance to $\Phi_{\mathrm{abs,tip,n}}$ at the tip of the hole. The corresponding ablation leads to a hole depth which is increased by the amount $z_{abl,n}$ from $z_{\mathrm{hole,n-1}}$ to $z_{\mathrm{hole,n}}$

$$\Phi_{\mathrm{abs},0} = \frac{A \cdot 2 \cdot E_p}{\pi \cdot w_0^2} \tag{3}$$

where $A$ is the material-specific absorptivity at normal incidence of a beam on a flat surface. The absorbed ablation threshold fluence $\Phi_{\mathrm{abs,th}}$ can be calculated by

$$\Phi_{\mathrm{abs,th}} = l_{\mathrm{ep}} \cdot h_{\mathrm{V,solid-vap}}, \tag{4}$$

where $l_{\mathrm{ep}}$ is the effective penetration depth of the laser beam and $h_{V,solid\text{-}vap}$ is the volume-specific enthalpy required for the complete vaporization of the material. The effective penetration depth $l_{ep}$ describes the energy transport into the material and is dominated by either the optical penetration depth or electron heat diffusion length depending on the peak fluence [26]. The ablation threshold fluence decreases with increasing number of pulses, also known as incubation effect. The threshold fluence depends on the material-specific incubation coefficient and is lowered by a factor of three to four from single pulses to several hundred pulses. As a result, the lowered ablation threshold causes an increased hole radius according to Eq. (2). For more than $10^3$ pulses, a saturation of the incubation effect occurs and the ablation threshold fluence is not decreased by further number of pulses [10]. For the sake of simplicity, the absorbed ablation threshold fluence $\Phi_{abs,th}$ is assumed to be constant over the entire drilling process in our model. When considering a drilling process of several tens of thousands pulses as shown in Fig. 2, the error caused by this simplification is negligible.

As explained in Fig. 3, the application of the $n^{\mathrm{th}}$ pulse in the conically shaped hole leads to the ablation of the yellow (horizontally) hatched material. By this, the hole depth is increased by the amount $z_{\mathrm{abl,n}}$ from $z_{\mathrm{hole,n-1}}$ to $z_{\mathrm{hole,n}}$. For the calculation of the depth increment $z_{\mathrm{abl,n}}$ achieved by the $n^{\mathrm{th}}$ pulse only the absorbed fluence $\Phi_{\mathrm{abs,tip,n}}$ reaching the tip of the conical hole is considered. The absorbed energy in the material volume exponentially drops with the distance to the sample surface, resulting in the logarithmic ablation law given by [27]

$$z_{\mathrm{abl,n}} = l_{\mathrm{ep}} \cdot \ln\left(\frac{\Phi_{\mathrm{abs,tip,n}}}{\Phi_{\mathrm{abs,th}}}\right) \tag{5}$$

Equation 5 holds for ablation of metals with laser pulses in the picosecond range when electron heat conduction is neglected [28]. Due to multiple reflections and diffuse scattering within the hole, the absorbed fluence at the tip $\Phi_{\mathrm{abs,tip,n}}$ cannot easily be determined, but raytracing simulations showed an elevated absorbed fluence near the tip of the hole [29]. Note that $\Phi_{\mathrm{abs,tip,n}}$ is the fluence at the tip of the hole resulting from the $n^{\mathrm{th}}$ pulse in the geometry of the hole as given after $n$-1 pulses, which has a depth of $z_{\mathrm{hole,n-1}}$. As the most simple approximation for an elevated

absorbed fluence near the tip of the hole, a linear increase of the absorbed fluence

$$\Phi(z)_{\mathrm{abs}} = \Phi_{\mathrm{abs,th}} + \left(\Phi_{\mathrm{abs,tip,n}} - \Phi_{\mathrm{abs,th}}\right) \cdot \frac{z}{z_{\mathrm{hole,n-1}}} \tag{6}$$

along the depth $z$ of the conically shaped hole is assumed, starting with the ablation threshold fluence $\Phi_{\mathrm{abs,th}}$ at the hole's opening and ending with the fluence $\Phi_{\mathrm{abs,tip,n}}$ at the hole's tip. This assumption is consistent with the fact that the regular drilling process gradually slows down with increasing depth, reaching a final limit when the absorbed fluence is reduced to the threshold value everywhere on the hole's wall as already presented in [16]. The superimposed increase of the hole's depth beyond the contribution of the regular process (as noticeable in phase 2 and 3) may be attributed to local irregularities in the hole's geometry generating more or less random hot spots of the incident radiation by multiple reflections in the hole [30]. At this state of the process, the ablation only occurs at the location of these hot spots and not on the whole surface of the hole as caused by the regular process, leading to an irregular and less reproducible drilling process during phases 2 and 3. The irregular contributions to the depth growth are not considered by the present model.

As the integral of the absorbed fluence on the surface of the hole equals the total energy $\eta_{abs,n-1} \cdot E_p$ absorbed in the hole,

$$\int_0^{z_{hole,n-1}} \frac{2 \cdot \pi \cdot \sqrt{r_{\mathrm{hole}}^2 + z_{\mathrm{hole,n-1}}^2}}{z_{\mathrm{hole,n-1}}} \cdot r(z) \cdot \Phi(z)_{\mathrm{abs}} dz = \eta_{\mathrm{abs,n-1}} \cdot E_{\mathrm{p}} \tag{7}$$

where

$$r(z) = r_{\mathrm{hole}} - r_{\mathrm{hole}} \cdot \frac{z}{z_{\mathrm{hole,n-1}}} \tag{8}$$

$\Phi_{\mathrm{abs,tip,n}}$ is found to be

$$\Phi_{\mathrm{abs,tip,n}} = \frac{3 \cdot \eta_{\mathrm{abs,n-1}} \cdot E_{\mathrm{p}}}{\pi \cdot r_{\mathrm{hole}} \cdot \sqrt{r_{\mathrm{hole}}^2 + z_{\mathrm{hole,n-1}}^2}} - 2 \cdot \Phi_{\mathrm{abs,th}} \tag{9}$$

where $\eta_{\mathrm{abs,n-1}}$ represents the overall absorptance of the $n^{\mathrm{th}}$ pulse in the hole geometry that is present after the $(n\text{-}1)^{\mathrm{th}}$ pulse. The overall absorptance $\eta_{\mathrm{abs,n-1}}$ is calculated based on the model originally introduced by *Gouffé* [31, 32] with the corrections by *Hügel* and *Graf* [33] and is found to be

$$\eta_{abs,n-1} = A \frac{1 + (1 - A)\left(\sigma_{\mathrm{n-1}} - \frac{\Omega_{\mathrm{n-1}}}{2\pi}\right)}{A \cdot \left(1 - \sigma_{\mathrm{n-1}}\right) + \sigma_{\mathrm{n-1}}}, \tag{10}$$

where $\sigma_{\mathrm{n-1}}$ is the ratio of the area of the opening of the hole to the complete surface area of the hole including the opening, and $\Omega_{n-1}$ is the solid angle under which the opening is seen from the tip of the hole. For a conical hole geometry $\sigma_{n-1}$ is given by

$$\sigma_{\mathrm{n-1}} = \frac{1}{1 + \sqrt{1 + \frac{z_{\mathrm{hole,n-1}}^2}{r_{\mathrm{hole}}^2}}} \tag{11}$$

and the solid angle $\Omega_{n-1}$ is given by

$$\Omega_{\mathrm{n-1}} = 4 \cdot \pi \cdot \sin^2\left(\frac{1}{2} \arctan\left(\frac{r_{\mathrm{hole}}}{z_{\mathrm{hole,n-1}}}\right)\right) \tag{12}$$

It is noted that the model presented here requires only two generally known laser parameters, $E_p$ and $w_0$, and three material parameters, $A$, $l_{\mathrm{ep}}$ and $h_{\mathrm{V,\,solid\text{-}vap}}$, which were determined for different metals in [34] and [35].

## 4 Experimental verification

The model for the prediction of the depth progress during percussion drilling derived in Sect. 3 was compared to experimental results obtained by drilling in stainless steel with the setup outlined in Sect. 2. The hole radius and drilling progress were calculated from the given laser parameters, i.e., for a beam radius of $w_0 = 61$ µm, and for three different pulse energies ranging from 143 µJ to 412 µJ, which corresponds to irradiated peak fluences ranging from 2.4 J/cm$^2$ to 7.0 J/cm$^2$. The values published in [35] and for iron were used to calculate $h_{\mathrm{V,solid\text{-}vap}} = 61$ J/mm$^3$ and are summarized in Table 1. The absorptivity was taken as $A = 0.38$ [34]. The penetration depth $l_{\mathrm{ep}}$ was used as a fit parameter. The best agreement for the whole drilling process was achieved with $l_{\mathrm{ep}} = 20$ nm and yields an absorbed threshold fluence of $\Phi_{\mathrm{abs,th}} = 0.12$ J/cm$^2$ (see Eq. (4)). The fitted value of the penetration depth $l_{\mathrm{ep}} = 20$ nm was assumed to be constant and is consistent with published values of the optical penetration depth of 21 nm for iron in [34] and 20 nm for stainless steel in [26].

**Table 1** Material parameters for iron published in [35] and [36] used for calculating the volume-specific enthalpy required for complete vaporization of the material $h_{\mathrm{V,solid\text{-}vap}}$

| Material parameter | Value |
|---|---|
| Density | $7870\,\frac{kg}{m^3}$ [35] |
| Heat capacity for solid iron | $449\,\frac{J}{kg \cdot K}$ [35] |
| Melting temperature | 1811 K [35] |
| Latent heat of melting | $247\,\frac{kJ}{kg}$ [35] |
| Evaporation temperature | 3134 K [35] |
| Latent heat of vaporization | $6260\,\frac{kJ}{kg}$ [36] |

The calculated hole radius according to Eq. (2) for the different pulse energies yields 61 µm for 143 µJ, 69 µm for 243 µJ and 76 µm for 412 µJ, respectively. The calculated hole radii were verified using the microscope images of drilled holes with a number of pulses $> 10^3$ to neglect the increasing hole radius due to the lowered ablation threshold caused by the incubation effect within the first few hundreds of pulses, which is not taken into account by our model. The calculated hole radii are in good agreement with the measured hole radii of $63 \pm 4$ µm for 143 µJ, $71 \pm 4$ µm for 243 µJ and $73 \pm 3$ µm for 412 µJ.

The hole depth as a function of the number of pulses for the different pulse energies is shown in Fig. 4. The solid lines correspond to the OCT-measurements, and the dotted lines to the values calculated with the analytical model presented in Sect. 3.

The depth progress decreases with increasing number of pulses and stagnates when the fluence in the tip $\Phi_{\mathrm{abs,tip,n}}$ converges the ablation threshold $\Phi_{\mathrm{abs,th}}$ (cf. Equation (5)). It can be seen that both the depth progress and the maximum drilling depth increase with increasing pulse energy. Drilling with the highest investigated pulse energy $E_{\mathrm{p}} = 412$ µJ yields a maximum hole depth of $> 1.5$ mm. The measured depth and model predictions are in excellent agreement for the examined pulse energies. The model only describes the drilling progress achieved by the contribution of the regular drilling process. The calculated curves and assumptions made therefore coincide very well with the experimental result during the first phase, where the irregular contributions are still negligible. The minor deviations between the curves at low numbers of pulses might result from the inaccuracy of the depth measurement [24] or uncertainties regarding the material parameters used for the calculation, in particular the value for $l_{ep}$ which might differ in the beginning of the drilling process when the fluence is still far above the ablation threshold. Furthermore, an increased absorptivity was measured for surfaces covered with microstructures which occur after a few hundred pulses [37, 38] and which were also found on the bottom of drilled holes [39]. This might lead to a faster than calculated drilling progress during the beginning of the drilling process. The deviation between the experimental and the theoretically predicted hole depth after a large number of pulses, which is especially observed for high pulse energies, is attributed to the additional contribution by the irregular drilling process as from phase 2, which is presumably induced by local geometrical irregularities, which are not considered by the model. Also not considered in the model are other physical phenomena that can influence the drilling rate in ambient atmosphere, such as a saturated ablation plume [40] and material redeposition [41]. Laser radiation of subsequent pulses is absorbed in the ablation plume if the temporal distance of the irradiating pulses is smaller than the time required for dissipation of the plume. In our experiments with the pulse repetition rate of 21.4 kHz, the effect of the ablation plume is negligible as the propagation velocity of the ablation plume is typically in the range of several hundreds of meters per second [42, 43]. Material redeposition on the walls of the hole can influence

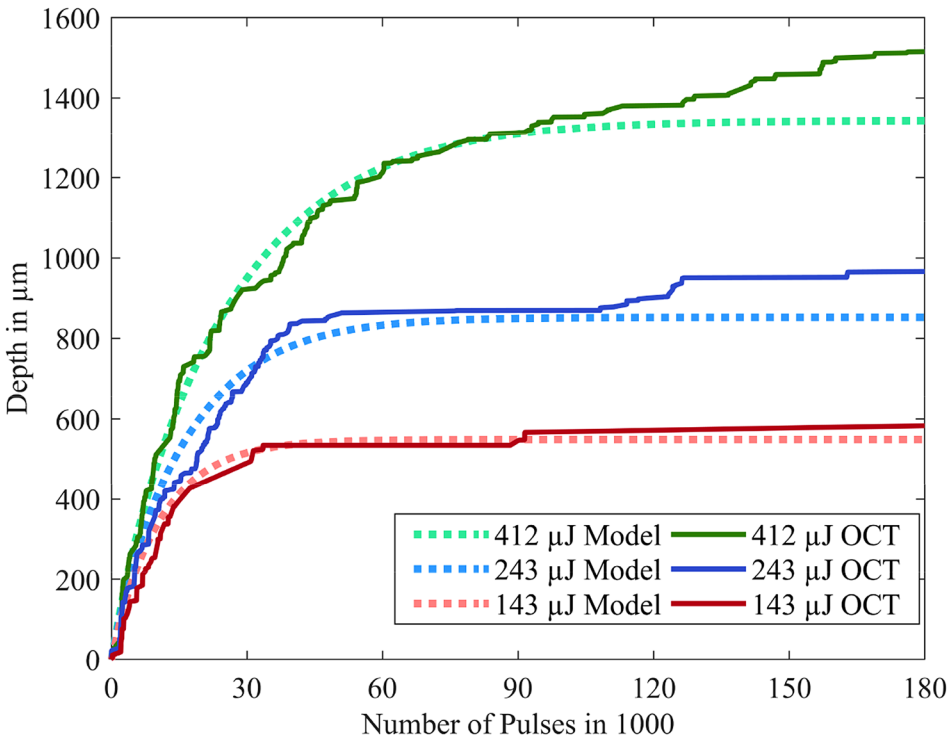


**Fig. 4** Hole depth as a function of the number of pulses for different pulse energies as measured by OCT (solid lines) and as predicted by the model derived in Sect. 3 (dotted lines). Parameters: $w_0 = 61$ µm, $A = 0.38$, $l_{\mathrm{ep}} = 20$ nm, $h_{\mathrm{V,solid\text{-}vap}} = 61$ J/mm$^3$ ($\Phi_{\mathrm{abs,th}} = 0.12$ J/cm$^2$)

the drilling rate [41] and hole geometry [44]. Geometrical deviations from the conical shape can also be caused by reflections from the walls of the hole resulting in a channel formation at the opening of the hole [45]. However, the conical hole shape clearly dominates the geometry of the drilled holes as shown by the cross sections in Fig. 2.

Hence, the investigations show that the presented model with the assumed conical hole geometry is suitable for the correct calculation of the hole radius and hole depth as achieved by the regular drilling process which dominates the first phase of percussion drilling. Knowing the absorptivity $A$, the effective penetration depth $l_{ep}$ and the evaporation enthalpy $h_{V,solid\text{-}vap}$ (or hence, $\Phi_{abs,th} = 0.12\ J/cm^2$), the pulse energy $E_p$ and the beam radius $w_0$, the model allows for the prediction of the depth of reproducible conical holes as a function of the applied number of pulses.

## 5 Conclusion

An analytical model for the prediction of the depth progress and hole depth of conically shaped holes which are percussion drilled in metals with ultrashort laser pulses was derived. The model predicts the progress of the drilling depth for percussion-drilled holes in stainless steel with picosecond pulses up to the quality depth limit. The corresponding assumptions for the model were experimentally validated for different laser parameters using OCT-based depth measurements and cross sections of the drilled holes.

**Acknowledgements** The authors thank Dr. Markus Kogel-Hollacher and Precitec for providing the OCT-based measurement system CHRocodile 2. Furthermore, the authors thank Liane Hoster for preparing the cross sections for the optical analysis and Dr. Lucy Blaney-Laible for proof-reading the manuscript.

**Funding** Open Access funding enabled and organized by Projekt DEAL. This work was partially funded by Federal Ministry for Economic Affairs and Energy (BMWi) on the basis of a decision by the German Bundestag (contract number ZF4592402FH8) and the German Research Foundation (DFG) under Grant No. GR 3172/21–1.

## Declarations

**Conflict of interest** The authors declare no conflicts of interest.



## References

1. F. Vollertsen, F. Schmidt, Int. J. Precis. Eng Manuf-Green Tech. **1**(1), 59–62 (2014)
2. E. Zahedi, C. Woerz, G. Reichardt, G. Umlauf, M. Liewald, J. Barz, R. Weber, D.J. Foerster, T. Graf, Manufacturing Rev. **6**, 11 (2019)
3. A. Feuer, C. Kunz, M. Kraus, V. Onuseit, R. Weber, T. Graf, D. Ingildeev, F. Hermanutz, in *Laser Applications in Microelectronic and Optoelectronic Manufacturing (LAMOM) XIX*, ed. by Y. Nakata, X. Xu, S. Roth, B. Neuenschwander (SPIE, 2014), 89670H
4. M. Kraus, M. Abdou Ahmed, A. Michalowski, A. Voss, R. Weber, T. Graf, Optics Express **18**, 22305 (2010)
5. H. Zhang, J. Di, M. Zhou, Y. Yan, R. Wang, Appl. Phys. A **119**, 745 (2015)
6. A. Kroschel, A. Michalowski, T. Graf, Adv. Opt. Technol. **7**, 183 (2018)
7. A. Ancona, F. Röser, K. Rademaker, J. Limpert, S. Nolte, A. Tünnermann, Opt. Express **16**, 8958 (2008)
8. J. Finger, M. Reininghaus, Opt. Express **22**, 18790 (2014)
9. T.V. Kononenko, C. Freitag, D.N. Sovyk, A.B. Lukhter, K.V. Skvortsov, V.I. Konov, Opt. Lasers Eng. **103**, 65 (2018)
10. F. Di Niso, C. Gaudiuso, T. Sibillano, F.P. Mezzapesa, A. Ancona, P.M. Lugarà, Opt. Express **22**, 12200 (2014)
11. D.J. Förster, R. Weber, T. Graf, Proceedings of LPM2018, 1 (2017)
12. R. Weber, T. Graf, P. Berger, V. Onuseit, M. Wiedenmann, C. Freitag, A. Feuer, Opt. Express **22**, 11312 (2014)
13. R. Weber, T. Graf, C. Freitag, A. Feuer, T. Kononenko, V.I. Konov, Opt. Express **25**, 3966 (2017)
14. S.M. Klimentov, T.V. Kononenko, P.A. Pivovarov, S.V. Garnov, V.I. Konov, A.M. Prokhorov, D. Breitling, F. Dausinger, Quantum Electron. **31**, 378 (2001)
15. S.M. Klimentov, S.V. Garnov, V.I. Konov, T.V. Kononenko, P.A. Pivovarov, O.G. Tsarkova, D. Breitling, F. Dausinger, Phys. Wave Phen. **15**, 1 (2007)
16. D.J. Förster, R. Weber, D. Holder, T. Graf, Opt. Express **26**, 11546 (2018)
17. S. Döring, S. Richter, S. Nolte, A. Tünnermann, Opt. Express **18**, 20395 (2010)
18. A. Gruner, J. Schille, U. Loeschner, Phys. Procedia **83**, 157 (2016)
19. W. Zhao, H. Liu, X. Shen, L. Wang, X. Mei, Materials (Basel, Switzerland) **13** (2019)
20. S. Döring, S. Richter, A. Tünnermann, S. Nolte, Appl. Phys. A **105**, 69 (2011)
21. D. Holder, A. Leis, M. Buser, R. Weber, T. Graf, Adv Opt Technol **9**, 101 (2020)
22. D. Holder, M. Buser, S. Boley, R. Weber, T. Graf, Mater. Des. **203**, 109567 (2021)
23. P.J.L. Webster, J.X.Z. Yu, B.Y.C. Leung, M.D. Anderson, V.X.D. Yang, J.M. Fraser, Opt. Lett. **35**, 646 (2010)
24. P.J.L. Webster, B.Y.C. Leung, J.X.Z. Yu, M.D. Anderson, T.P. Hoult, J.M. Fraser, In *Micromachining and Microfabrication Process Technology XV*, ed. by M.A. Maher, J.-C. Chiao, P.J. Resnick (SPIE, 2010), 759003
25. J.M. Liu, Opt. Lett. **7**, 196 (1982)
26. P.T. Mannion, J. Magee, E. Coyne, G.M. O'Connor, T.J. Glynn, Appl. Surf. Sci. **233**, 275 (2004)

27. B. Neuenschwander, B. Jaeggi, M. Schmid, G. Hennig, Phys. Procedia **56**, 1047 (2014)
28. B.N. Chichkov, C. Momma, S. Nolte, F. von Alvensleben, A. Tünnermann, Appl. Phys. A **63**, 109 (1996)
29. A. Michalowski, Y. Qin, R. Weber, T. Graf, in *Laser Sources and Applications II*, ed. by J.I. Mackenzie, H. JelÍnková, T. Taira, M. Abdou Ahmed (SPIE, 2014), 91350R
30. S. Döring, *Analysis of the Hole Shape Evolution in Ultrashort Pulse Laser Drilling* (Cuvillier Verlag, Jena, 2014).
31. A. Gouffé, Revue d'Optique **24**, 1 (1945)
32. A. Gouffé, *Aperture Corrections of Artificial Black Bodies with Consideration of Multiple Internal Diffusions* (San Diego, CA, 1960).
33. H. Hügel, T. Graf, *Laser in Der Fertigung: Strahlquellen, Systeme, Fertigungsverfahren: Strahlquellen, Systeme, Fertigungsverfahren* (Vieweg+Teubner Verlag, Wiesbaden, 2014).
34. P.B. Johnson, R.W. Christy, Phys. Rev. B **9**, 5056 (1974)
35. D.R. Lide, *CRC Handbook of Chemistry and Physics* (CRC Press/Taylor and Francis, Boca Raton, FL, 2010).
36. G.W.C. Kaye, T.H. Laby, *Tables of Physical & Chemical Constants* (Longman, Harlow, 1995).
37. P. Gecys, A. Vinciunas, M. Gedvilas, A. Kasparaitis, R. Lazdinas, G. Raciukaitis, JLMN **10**, 129 (2015)
38. D.H. Kam, J. Mazumder, J. Kim, J. Laser Appl. **28**, 42001 (2016)
39. P.S. Banks, M.D. Feit, A.M. Rubenchik, B.C. Stuart, M.D. Perry, Appl. Phys. A **69**, 377 (1999)
40. E.G. Gamaly, N.R. Madsen, M. Duering, A.V. Rode, V.Z. Kolev, B. Luther-Davies, Phys. Rev. B **71**, 1051 (2005)
41. A. Weck, T.H.R. Crawford, D.S. Wilkinson, H.K. Haugen, J.S. Preston, Appl. Phys. A **90**, 537 (2008)
42. J.F. Düsing, D.J. Hwang, C.G. Grigoropoulos, A. Ostendorf, R. Kling, International Congress on Applications of Lasers & Electro Optics (ICALEO), 888 (2009)
43. J. Winter, S. Rapp, M. Spellauge, C. Eulenkamp, M. Schmidt, H.P. Huber, Appl. Surf. Sci. **511**, 145514 (2020)
44. A. Luft, U. Franz, A. Emsermann, J. Kaspar, Appl. Phys. A **63**, 93 (1996)
45. K.-W. Park, S.-J. Na, Appl. Surf. Sci. **256**, 2392 (2010)